Joint Beamforming for NLOS Target Detection with RIS-Assisted Radar in Multipath Environments

Cengcang Zeng, and Hongbin Li
Department of Electrical and Computer Engineering
Stevens Institute of Technology
Hoboken, NJ 07030, USA

***Abstract*—Reconfigurable intelligent surfaces (RIS) have gained prominence in communications and are now extending their applications to radar, offering innovative solutions for non-line-of-sight (NLOS) target detection. This paper introduces a new joint transmit and RIS beamforming approach for NLOS target detection using RIS-assisted radar systems operating in multipath environments. Leveraging manifold-based optimization, the proposed method jointly optimizes the radar's active beamformer and the RIS phase shifts to enhance detection robustness by managing the interference and signal degradation caused by multipath propagation. We provide a detailed analysis of detection performance, including the probability of detection and probability of false alarm, to assess the effectiveness of the approach. The proposed method is further compared with a conventional approach that focuses solely on the line-of-sight (LOS) component of the multipath signals. While the conventional method performs comparably in scenarios with a strong dominant LOS path, the proposed approach demonstrates notably superior performance across more general multipath environments. Simulation results underscore the applicability of the proposed method, particularly in environments with high angular spread, highlighting RIS's potential for improved detection in complex, multipath-dense settings where traditional approaches may be limited.**

***Index Terms*—Non-line-of-sight (NLOS) target detection, reconfigurable intelligent surface (RIS), joint beamforming, multipath**

I. Introduction

Reconfigurable intelligent surfaces (RIS) are gaining attention as a transformative technology in RF sensing and wireless communication [1]–[5], offering flexible control over electromagnetic wave propagation to improve signal processing and target detection. By dynamically adjusting properties such as phase, amplitude, and polarization, RIS enhances radar and network performance, especially in complex, multipath environments [6]. This adaptability is essential in non-line-of-sight (NLOS) scenarios, often found in urban settings, where RIS can adjust signal paths to mitigate obstacles and reduce degradation [7]. Studies highlight RIS's potential to improve detection and tracking for RF sensing applications like autonomous driving and smart cities, where high accuracy in detection and localization is critical [8]. The integration of RIS with RF sensing also supports the demands of next-generation wireless technologies [9].

This work was supported in part by the National Science Foundation under grants CCF-2316865, ECCS-1923739, ECCS-2212940, and ECCS-23325341.

The application of RIS has expanded beyond communications into radar systems, where it plays a crucial role in line-of-sight (LOS) and NLOS target detection [10]–[12]. In radar, RIS can reflect signals around obstacles, enhancing target detection in cluttered environments [13], [14]. To address timing mismatches, recent studies have examined asynchronous propagation management in RIS-assisted RF sensing [15]. Additionally, RIS has been integrated into dual-function radar and communication (DFRC) systems to improve interference mitigation, detection sensitivity, and adaptive beamforming in complex scenarios [16], [17].

Although RIS-assisted radar has been explored in various studies, much of the existing work focuses on single-path scenarios [14], [18], [19], limiting its applicability in real-world, multipath-rich environments. Most approaches aim solely to enhance direct LOS paths for detection accuracy in simple LOS settings, without addressing the complexities of multipath propagation. In urban and indoor environments, signals frequently undergo multiple reflections, leading to indirect NLOS paths that introduce interference and phase misalignment [20]. Traditional methods fall short in these settings, underscoring the need for approaches that address both LOS and multipath effects to ensure robust detection in cluttered, obstructed scenarios.

In this paper, we introduce a novel joint transmit and RIS beamforming approach for RIS-assisted radar systems that is tailored for multipath-rich environments. Our framework models both LOS and NLOS paths, addressing the complexities of multipath propagation. This joint optimization is aimed at maximizing received signal power and enhancing detection robustness by mitigating the interference and degradation associated with NLOS paths. To evaluate the effectiveness of the proposed method, we analyze key detection metrics, including the probability of detection and probability of false alarm, and compare the approach against a conventional method that focuses solely on the LOS path. While the conventional approach performs adequately in scenarios with a dominant LOS path, our proposed method consistently outperforms it in diverse multipath environments, especially under conditions of high angular spread. These findings highlight the robustness and adaptability of RIS in complex environments, offering practical solutions for radar applications in multipath-rich NLOS scenarios. Simulation results underscore the adaptability of the proposed approach, demonstrating its potential to

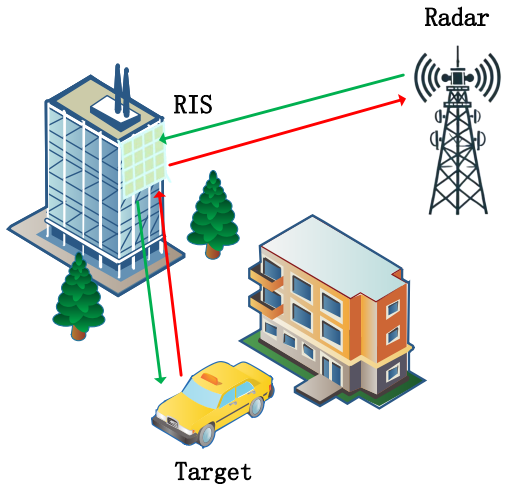

Figure 1. A mono-static radar with an RIS employed to assist NLOS target illumination and observation.

significantly improve detection performance in settings where traditional methods are often limited.

II. Signal Model

In this paper, we explore a mono-static RIS-assisted radar system for NLOS target detection, focusing on realistic scenarios where multi-path signal propagation occurs, as illustrated in Fig.,1. The RIS is strategically positioned to enhance both target illumination and signal reflection back to the radar, which is equipped with N transmit/receive antennas. The RIS consists of M meta-atoms, each of which introduces an independent phase shift ψ_m. The overall phase response of the RIS can be expressed as:

$$\boldsymbol{\Psi} = \text{diag}(\boldsymbol{\psi}), \tag{1}$$

where $\boldsymbol{\psi} = [\psi_1, \cdots, \psi_M]^T$ with $|\psi_m| = 1$.

In comparison to conventional single path models, we consider a more realistic scenario involving multiple propagation paths between the radar, RIS, and the target. These paths include both LOS and NLOS paths due to reflections and diffractions caused by obstacles in the environment. The received signal at the radar, after matched filtering and sampling, is given by:

$$z = \alpha\sqrt{P_{\text{t}}}\boldsymbol{w}^T\boldsymbol{H}_{\text{r,s}}^T\boldsymbol{\Psi}\boldsymbol{h}_{\text{s,a}}\boldsymbol{h}_{\text{s,a},k}^T\boldsymbol{\Psi}\boldsymbol{H}_{\text{r,s},l}\boldsymbol{w} + \epsilon, \tag{2}$$

where α is the complex target reflection coefficient, $\boldsymbol{w}$ is the unit-norm transmit beamforming vector, and ϵ represents the Gaussian noise with variance σ_n^2.

The radar-RIS and RIS-target channels are modeled as sums over multiple paths. The radar-RIS channel for the l-th path is defined as:

$$\boldsymbol{H}_{\text{r,s}} = \sum_{l=0}^{L_{\text{r,s}}-1} \boldsymbol{H}_{\text{r,s},l} = \sum_{l=0}^{L_{\text{r,s}}-1} \rho_{\text{r,s},l}\boldsymbol{a}_{\text{s}}(\boldsymbol{\phi}_{\text{r,s},l})\boldsymbol{a}_{\text{t}}^H(\boldsymbol{\theta}_{\text{r,s},l}), \tag{3}$$

where $l = 0$ represents the LOS path, and $l > 0$ represents the additional NLOS paths due to reflections. Similarly, the RIS-target channel is given by:

$$h_{\text{s,a}} = \sum_{k=0}^{L_{\text{s,a}}-1} \boldsymbol{h}_{\text{s,a},k} = \sum_{k=0}^{L_{\text{s,a}}-1} \rho_{\text{s,a},k}\boldsymbol{a}_{\text{s}}^*(\boldsymbol{\theta}_{\text{s,a},k}), \tag{4}$$

with $k = 0$ denoting the LOS path, and $k > 0$ accounting for the multiple reflections between the RIS and the target.

In this model, the steering vectors $\boldsymbol{a}_{\text{r}}(\boldsymbol{\theta}), \boldsymbol{a}_{\text{s}}(\boldsymbol{\theta})$, and $\boldsymbol{a}_{\text{s}}(\boldsymbol{\phi})$ represent the radar transmit steering vector, RIS steering vector for the angle of departure (AoD) $\boldsymbol{\theta}$, and RIS steering vector for the angle of arrival (AoA) $\boldsymbol{\phi}$, respectively. These vectors capture the beamforming characteristics of both the radar and RIS.

The path gains $\rho_{\text{r,s},l}$ and $\rho_{\text{s,a},k}$ reflect critical factors like distance, antenna gain, and propagation losses across the radar-RIS and RIS-target links, with total path loss accounting for transmission losses, atmospheric effects, and other signal degradation. Each path contributes unique phase and amplitude shifts, which add complexity to beamforming design and require collective optimization to enhance received signal power.

This multi-path model significantly increases the complexity of the beamforming design, as each path contributes a phase and amplitude shift that must be taken into account to maximize the received signal power. The contributions of both LOS and NLOS paths necessitate a joint optimization of the radar beamforming vector $\boldsymbol{w}$ and the RIS phase matrix $\boldsymbol{\Psi}$ to improve detection performance in NLOS scenarios. By incorporating multiple paths, this approach models real-world challenges, such as reflections from buildings and other structures, that affect the propagation of signals in urban and cluttered environments. This stands in contrast to traditional single-path models, which oversimplify the complexities involved in NLOS target detection.

III. Joint Radar and RIS Beamforming Design

This section discusses the joint optimization of the radar beamformer $\boldsymbol{w}$ and the RIS phase matrix $\boldsymbol{\Psi}$ in multipath scenarios, with the objective of maximizing received signal power. Two methods are presented: a conventional approach that optimizes based on the direct LOS path and a manifold-based approach designed to mitigate the effects of multipath-induced distortions.

The radar beamformer is optimized to maximize target illumination power, which is proportional to $\|\boldsymbol{h}_{\text{s,a}}^T\boldsymbol{\Psi}\boldsymbol{H}_{\text{r,s}}\boldsymbol{w}\|^2$. The optimization problem for $\boldsymbol{w}$ can be formulated as:

$$\begin{aligned} \widetilde{\boldsymbol{w}} = \arg \max_{\boldsymbol{w}} \quad & \left\|\boldsymbol{h}_{\text{s,a}}^T\boldsymbol{\Psi}\boldsymbol{H}_{\text{r,s}}\boldsymbol{w}\right\|^2 \\ \text{s.t.} \quad & \|\boldsymbol{w}\|^2 = 1. \end{aligned} \tag{5}$$

The optimal solution for the radar beamformer $\boldsymbol{w}$ is the principal eigenvector of the matrix $\boldsymbol{H}_{\mathrm{r,s}}^H \boldsymbol{\Psi}^H \boldsymbol{h}_{\mathrm{s,a}}^* \boldsymbol{h}_{\mathrm{s,a}}^T \boldsymbol{\Psi} \boldsymbol{H}_{\mathrm{r,s}}$, and is given by:

$$\widetilde{\boldsymbol{w}} = \frac{\boldsymbol{H}_{\mathrm{r,s}}^H \boldsymbol{\Psi}^H \boldsymbol{h}_{\mathrm{s,a}}^*}{\|\boldsymbol{H}_{\mathrm{r,s}}^H \boldsymbol{\Psi}^H \boldsymbol{h}_{\mathrm{s,a}}^*\|}, \tag{6}$$

which is a matched transmission filter that is matched to the effective channel.

With $\boldsymbol{w}$ optimized, the next focus is on refining detection performance through RIS phase shift optimization. The total received signal power, incorporating both LOS and NLOS paths, is represented as:

$$\|\boldsymbol{H}_{\mathrm{r,s}}^H \boldsymbol{\Psi}^H \boldsymbol{h}_{\mathrm{s,a}}^*\|^4 = \left\| \boldsymbol{\psi}^T \sum_{l=0}^{L_{\mathrm{s,a}}-1} \sum_{k=0}^{L_{\mathrm{r,s}}-1} \rho_{\mathrm{s,a},l} \rho_{\mathrm{r,s},k} \times \mathrm{diag}(\boldsymbol{a}_{\mathrm{s}}(\boldsymbol{\theta}_{\mathrm{s,a},l})) \boldsymbol{a}_{\mathrm{s}}(\boldsymbol{\phi}_{\mathrm{r,s},k}) \boldsymbol{a}_{\mathrm{t}}^H(\boldsymbol{\theta}_{\mathrm{r,s},k}) \right\|^4, \tag{7}$$

where the 4th-order exponent is due to matched transmission and the round-trip propagation of the signal.

The following subsections present the two optimization strategies for $\boldsymbol{\psi}$: a conventional approach that aligns RIS phase shifts primarily with the direct LOS path, and a manifold-based approach that aims to counteract the distortions introduced by multipath propagation.

A. Conventional Approach

In the conventional approach, the RIS phase vector $\boldsymbol{\psi}$ is optimized specifically for the dominant LOS path, disregarding NLOS path contributions. This approach simplifies the optimization by focusing solely on LOS-path alignment, which is computationally efficient but suboptimal in multipath-dominant environments.

The RIS phase vector can thus be expressed as:

$$\widetilde{\boldsymbol{\psi}} = \left[e^{-j \arg(s_1)}, \cdots, e^{-j \arg(s_M)} \right]^T, \tag{8}$$

where $\boldsymbol{s} = \boldsymbol{a}_{\mathrm{s}}^*(\boldsymbol{\theta}_{\mathrm{s,a}}) \odot \boldsymbol{a}_{\mathrm{s}}(\boldsymbol{\phi}_{\mathrm{r,s}})$ and s_m represents the m-th entry of the steering vector $\boldsymbol{s}$ for the LOS path. This approach provides acceptable detection performance in scenarios where the LOS path is the primary contributor to the received signal power but may underperform in complex multipath environments.

B. Proposed Approach

The proposed approach leverages a manifold gradient descent method to optimize the RIS phase vector $\boldsymbol{\psi}$, considering both LOS and NLOS path contributions in multipath-rich environments. The objective is to maximize the received signal power by adjusting $\boldsymbol{\psi}$ on the complex circle manifold, where each element satisfies the unit-modulus constraint $|\psi_m| = 1$. The objective function can be expressed as:

$$f(\boldsymbol{\psi}) = \left\| \boldsymbol{\psi}^T \sum_{l=0}^{L_{\mathrm{s,a}}-1} \sum_{k=0}^{L_{\mathrm{r,s}}-1} \rho_{\mathrm{s,a},l} \rho_{\mathrm{r,s},k} \mathrm{diag}(\boldsymbol{a}_{\mathrm{s}}(\boldsymbol{\theta}_{\mathrm{s,a},l})) \times \boldsymbol{a}_{\mathrm{s}}(\boldsymbol{\phi}_{\mathrm{r,s},k}) \boldsymbol{a}_{\mathrm{t}}^H(\boldsymbol{\theta}_{\mathrm{r,s},k}) \right\|^2 = \left\| \boldsymbol{\psi}^T \mathbf{A} \right\|^2, \tag{9}$$

where

$$\mathbf{A} = \sum_{l=0}^{L_{\mathrm{s,a}}-1} \sum_{k=0}^{L_{\mathrm{r,s}}-1} \rho_{\mathrm{s,a},l} \rho_{\mathrm{r,s},k} \mathrm{diag}(\boldsymbol{a}_{\mathrm{s}}(\boldsymbol{\theta}_{\mathrm{s,a},l})) \boldsymbol{a}_{\mathrm{s}}(\boldsymbol{\phi}_{\mathrm{r,s},k}) \boldsymbol{a}_{\mathrm{t}}^H(\boldsymbol{\theta}_{\mathrm{r,s},k}). \tag{10}$$

The design problem can thus be formulated as

$$\begin{aligned} \max_{\boldsymbol{\psi}} \quad & f(\boldsymbol{\psi}) \\ \text{s.t.} \quad & |\psi_m| = 1, \quad \forall m = 1, \ldots, M. \end{aligned} \tag{11}$$

To address this optimization problem, we apply a manifold optimization technique tailored to handle the non-convex unit modulus constraint. In this approach, the search space can be regarded as the product of M complex circles S^M, where $S = \{u \in \mathbb{C} : u^H u = 1\}$ represents a unit circle in the complex plane [21]. The complex circle manifold, denoted as $\mathcal{M}$, is defined as

$$\mathcal{M} = S^M \triangleq \{\boldsymbol{\psi} \in \mathbb{C}^M : |\psi_m| = 1, \quad m = 1, \ldots, M\}.$$

A manifold gradient descent approach is then employed to ensure that the optimization respects the unit-modulus constraint, following three main steps [22], [23]: gradient projection, descent, and retraction.

The optimization process begins by calculating the gradient of the objective function $f(\boldsymbol{\psi})$ with respect to $\boldsymbol{\psi}$. To obtain a feasible search direction, this gradient is projected onto the tangent space $T_{\boldsymbol{\psi}_{(i)}}\mathcal{M}$ of the complex circle manifold [21], where

$$T_{\boldsymbol{\psi}_{(i)}}\mathcal{M} = \{\boldsymbol{z} \in \mathbb{C}^M : \mathrm{Re}\{z \odot \boldsymbol{\psi}_{(i)}\} = \mathbf{0}\}, \tag{12}$$

and $\mathrm{Re}(\cdot)$ extracts the real part. The i-th iteration of the optimization process ensures adherence to the manifold's constraints. Specifically, the search direction is calculated as:

$$\boldsymbol{\eta}_{(i)} = -\nabla_{\boldsymbol{\psi}_{(i)}} f(\boldsymbol{\psi}) = -2\mathbf{A}^H \mathbf{A} \boldsymbol{\psi}_{(i)}, \tag{13}$$

where $\nabla_{\boldsymbol{\psi}} f(\boldsymbol{\psi})$ denotes the gradient of f with respect to $\boldsymbol{\psi}$, and the projection operator $\mathrm{Proj}_{T_{\boldsymbol{\psi}_{(i)}}\mathcal{M}}(\cdot)$ of $\boldsymbol{\eta}_{(i)}$ is defined as:

$$\mathrm{Proj}_{T_{\boldsymbol{\psi}_{(i)}}\mathcal{M}}(\boldsymbol{\eta}_{(i)}) = \boldsymbol{\eta}_{(i)} - \mathrm{Re}\{\boldsymbol{\eta}_{(i)}^* \odot \boldsymbol{\psi}_{(i)}\} \odot \boldsymbol{\psi}_{(i)}, \tag{14}$$

This projection operation ensures that $\boldsymbol{\eta}_{(i)}$ lies within the tangent space of the manifold, preserving the unit-modulus constraint for each element.

Following the projection step, the phase vector $\boldsymbol{\psi}_{(i)}$ is updated by moving along the projected gradient direction $P_{T_{\boldsymbol{\psi}_{(i)}}\mathcal{M}}(\boldsymbol{\eta}_{(i)})$ with a step size β, resulting in a temporary update:

$$\tilde{\boldsymbol{\psi}}_{(i)} = \boldsymbol{\psi}_{(i)} + \beta \mathrm{Proj}_{T_{\boldsymbol{\psi}_{(i)}}\mathcal{M}}(\boldsymbol{\eta}_{(i)}). \tag{15}$$

To ensure the updated vector satisfies the unit-modulus constraint, a retraction operation maps $\tilde{\boldsymbol{\psi}}_{(i)}$ back onto the complex circle manifold by normalizing each element:

$$\boldsymbol{\psi}_{(i+1)} = \text{Ret}(\tilde{\boldsymbol{\psi}}_{(i)}) = \tilde{\boldsymbol{\psi}}_{(i)} \odot \frac{1}{\left|\tilde{\boldsymbol{\psi}}_{(i)}\right|}, \tag{16}$$

where $\frac{1}{|\tilde{\boldsymbol{\psi}}_{(i)}|} \triangleq \left[|\tilde{\psi}_{1,(i)}|^{-1}, \cdots, |\tilde{\psi}_{M,(i)}|^{-1}\right]^T$. This retraction guarantees that each component of $\boldsymbol{\psi}_{(i+1)}$ remains on the complex unit circle, maintaining the feasibility of the solution within the manifold constraints.

The manifold gradient descent algorithm iterates through these steps until a convergence criterion is met, typically defined by a small tolerance κ on the change in $f(\boldsymbol{\psi})$:

$$\left| f(\boldsymbol{\psi}_{(i+1)}) - f(\boldsymbol{\psi}_{(i)}) \right| \leq \kappa. \tag{17}$$

By iteratively refining $\boldsymbol{\psi}$, the proposed method adapts to multipath conditions, demonstrating robustness and improved detection performance in complex, multipath-dense scenarios.

In summary, this manifold optimization of $\boldsymbol{\psi}$ effectively addresses the limitations of conventional LOS-focused methods, offering substantial performance improvements in multipath-rich NLOS environments.

IV. Target Detection

We now turn to the problem of NLOS target detection in the RIS-assisted radar system. The received signal, after applying the optimal radar beamformer $\widetilde{\boldsymbol{w}}$ and the optimized RIS phase vector $\widetilde{\boldsymbol{\psi}}$, simplifies to:

$$z = \alpha\sqrt{P_\text{t}}\|\boldsymbol{H}_\text{r,s}^H \widetilde{\boldsymbol{\Psi}}^H \boldsymbol{h}_\text{s,a}^*\|^2 + \epsilon, \tag{18}$$

where ϵ is the noise term. The task of target detection is then formulated as a binary hypothesis testing problem with two hypotheses:

$$\begin{aligned} &\mathcal{H}_0 : z = \epsilon, \\ &\mathcal{H}_1 : z = \alpha\sqrt{P_\text{t}}\|\boldsymbol{H}_\text{r,s}^H \widetilde{\boldsymbol{\Psi}}^H \boldsymbol{h}_\text{s,a}^*\|^2 + \epsilon, \end{aligned} \tag{19}$$

where $\mathcal{H}_0$ corresponds to the absence of the target, and $\mathcal{H}_1$ corresponds to the presence of the target.

To solve this hypothesis testing problem, we employ a simple detection scheme where the test statistic is defined as:

$$T = |z| \underset{\mathcal{H}_0}{\overset{\mathcal{H}_1}{\gtrless}} \gamma. \tag{20}$$

with γ as the decision threshold.

Under $\mathcal{H}_0$, the received signal z is modeled as a complex Gaussian random variable with zero mean and variance σ_n^2, i.e., $z \sim \mathcal{CN}(0, \sigma_n^2)$. Consequently, the test statistic T follows a Rayleigh distribution, and its probability density function (PDF) is given by:

$$p_T(t|\mathcal{H}_0) = \frac{2t}{\sigma_n^2} e^{-\frac{t^2}{\sigma_n^2}}, \ t \geq 0. \tag{21}$$

Under $\mathcal{H}_1$, z is a complex Gaussian random variable with a non-zero mean $\alpha\sqrt{P\text{t}}\|\boldsymbol{H}_\text{r,s}^H \widetilde{\boldsymbol{\Psi}}^H \boldsymbol{h}_\text{s,a}^*\|^2$ and the same variance σ_n^2. In this case, the real and imaginary parts of z are normally distributed as:

$$\Re\{z\} \sim \mathcal{N}(\Re\{\alpha\sqrt{P_\text{t}}\|\boldsymbol{H}_\text{r,s}^H \widetilde{\boldsymbol{\Psi}}^H \boldsymbol{h}_\text{s,a}^*\|^2, \sigma_n^2/2) \tag{22}$$

and similarly for the imaginary part. Therefore, the test statistic T follows a Rician distribution, and its PDF under $\mathcal{H}_1$ is given by:

$$p_T(t|\mathcal{H}_1) = \frac{2t}{\sigma_n^2} e^{-\frac{1}{\sigma_n^2}(t^2+\beta^2)} I_0\Big(\frac{2\beta t}{\sigma_n^2}\Big), \ t \geq 0, \tag{23}$$

where $\beta^2 = |\alpha|^2 P_\text{t}\|\boldsymbol{H}_\text{r,s}^H \widetilde{\boldsymbol{\Psi}}^H \boldsymbol{h}_\text{s,a}^*\|^4$ and $I_0(\cdot)$ is the modified Bessel function of the first kind.

To evaluate the detection performance, the false alarm probability (P_f) is calculated as:

$$P_f = \int_\gamma^\infty p_T(t|\mathcal{H}_0)dt = e^{\frac{-\gamma^2}{\sigma_n^2}}. \tag{24}$$

The detection threshold γ can thus be expressed in terms of the desired false alarm probability:

$$\gamma = \sqrt{-\sigma_n^2 \ln P_f}. \tag{25}$$

Similarly, the probability of detection (P_d) is obtained as:

$$\begin{aligned} P_d &= \int_\gamma^\infty p_T(t|\mathcal{H}_1)dt \\ &= \int_\gamma^\infty \frac{2t}{\sigma_n^2} e^{-\frac{1}{\sigma_n^2}(t^2+\beta^2)} I_0\Big(\frac{2\beta t}{\sigma_n^2}\Big) \\ &= Q\left(\sqrt{\frac{2|\alpha|^2 P_\text{t}\|\boldsymbol{H}_\text{r,s}^H \widetilde{\boldsymbol{\Psi}}^H \boldsymbol{h}_\text{s,a}^*\|^4}{\sigma_n^2}}, \sqrt{\frac{2\gamma^2}{\sigma_n^2}}\right). \end{aligned} \tag{26}$$

where $Q(\cdot,\cdot)$ is the generalized Marcum Q-function.

V. Numerical Results

In this section, we present simulation results to evaluate the impact of RIS on detection performance in multipath environments. The simulation models a mono-static RIS-assisted radar setup with both LOS and NLOS paths, illustrating the effect of multipath contributions on detection. The radar is configured as a ULA with 64 antennas ($N = 64$), while the RIS is a UPA with $M = N_x \times N_y$ meta-atoms. Key parameters include a target RCS of 0.02 m^2, carrier frequency of 10 GHz, noise variance $\sigma_n^2 = -90$ dBm, and a false alarm probability $P_f = 10^{-2}$. The SNR is defined as

$$\text{SNR} = \frac{|\alpha|^2 P_\text{t}\|\boldsymbol{H}_\text{r,s}^H \boldsymbol{h}_\text{s,a}^*\|^4}{\sigma_n^2}. \tag{27}$$

where $\rho_\text{r,s,0}$ and $\rho_\text{s,a,0}$ represent the LOS path gains for radar-RIS and RIS-target links.

To characterize the multipath environment, we use the Rician factor $K \triangleq \frac{|\rho_0|^2}{\sum_{l=1}^{L-1}|\rho_l|^2}$, which quantifies the energy ratio between the LOS and NLOS paths. In this mono-static NLOS radar system, the direct path represents the primary LOS component, with signals traveling from the radar to the

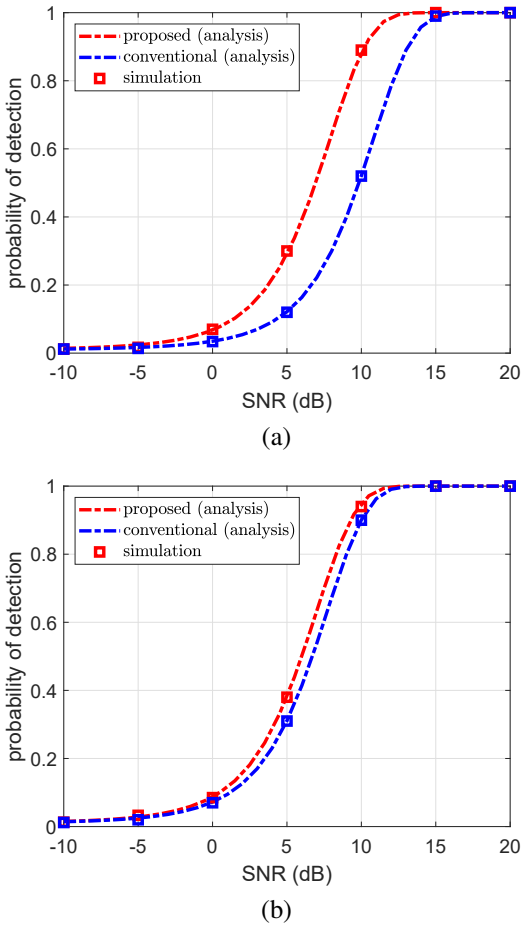

Figure 2. Detection performance in multipath scenarios (a) Strong multipath environment (b) LOS-dominant environment.

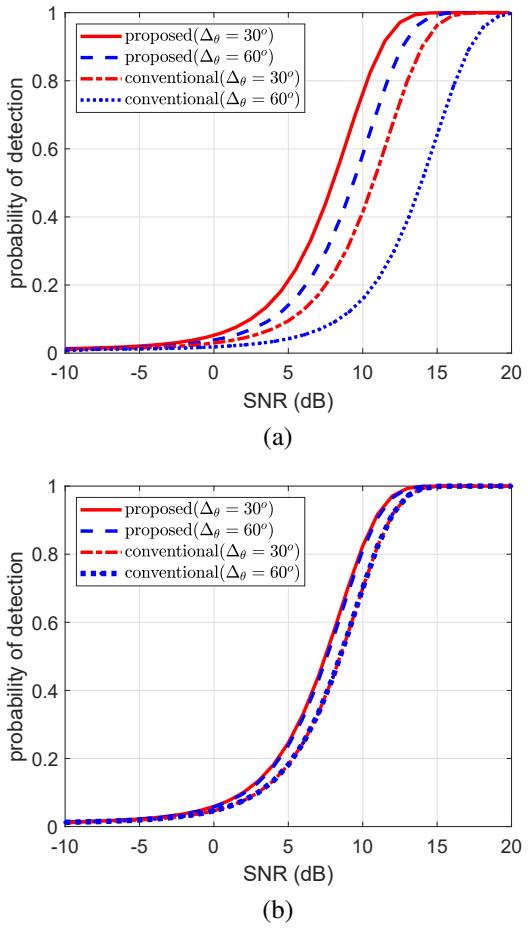

Figure 3. Detection performance under varying angle deviations (a) Strong multipath environment (b) LOS-dominant environment.

RIS and subsequently from the RIS to the target. In contrast, the indirect paths represent NLOS contributions, where signals experience multiple reflections or diffractions before reaching either the RIS or the target. In this paper, we set $K = 13.2$ dB to represent an LOS-dominant environment and $K = 0$ dB to represent a strong multipath environment. In the following results, we generally consider the number of paths $L = 3$ as the typical multipath scenario.

Figs. 2(a) and 2(b) present the detection performance in two distinct multipath conditions: strong multipath (NLOS-dominant) and LOS-dominant environments, respectively. In the strong multipath environment shown in Fig. 2(a), the proposed method significantly outperforms the conventional approach across various SNR levels, demonstrating robustness in complex NLOS conditions where NLOS paths introduce substantial interference and phase misalignment. This improved performance is attributed to the proposed method's ability to jointly optimize both LOS and NLOS path contributions, thereby effectively mitigating multipath-induced degradation. Conversely, in the LOS-dominant environment (Fig. 2(b)), the detection performance of both methods is nearly identical, indicating that when the LOS path is dominant and multipath

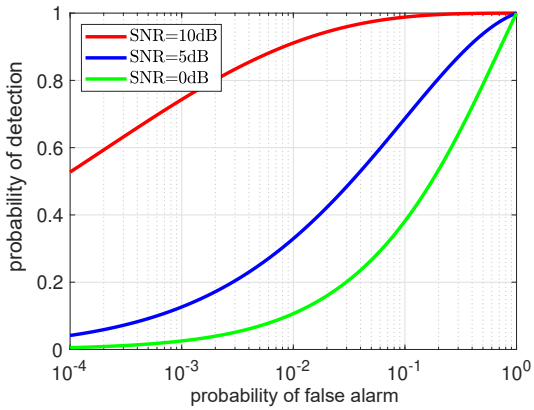

Figure 4. ROC Curves of the proposed method at different SNR levels in a strong multipath environment.

effects are minimal, the conventional method, which focuses primarily on the direct path, is sufficient for high detection accuracy. These findings align with the theoretical analysis in Section IV, validating the proposed method's advantage in complex multipath-dense settings and highlighting its ap-

plicability for challenging NLOS scenarios where traditional approaches may be limited.

Figs. 3(a) and 3(b) illustrate the impact of angle deviation (Δ_θ) of NLOS paths relative to the LOS path on detection performance in different multipath scenarios. In the strong multipath environment shown in Fig. 3(a), the proposed approach consistently outperforms the conventional method, particularly when the NLOS paths deviate significantly from the LOS direction (e.g., $\Delta_\theta = 60^\circ$). This result demonstrates the robustness of the proposed method in scenarios with high angular diversity, as it effectively mitigates the performance degradation caused by interference from widely spread NLOS paths. In contrast, Fig. 3(b), which depicts the LOS-dominant environment, shows that both the proposed and conventional methods achieve similar detection performance across different angle deviations. This outcome suggests that when the LOS path dominates, the influence of angular spread is minimal, making the conventional approach sufficient. These findings underscore the proposed method's advantage in complex multipath-dense environments, particularly those with significant angular spread among NLOS paths, where traditional methods may fall short.

Figure 4 illustrates the ROC curves of the proposed method under different SNR levels (0 dB, 5 dB, and 10 dB) in a strong multipath environment. As SNR increases, the detection probability P_d improves across all false alarm probabilities P_f. At 0 dB SNR, detection performance is limited, particularly at low P_f, due to noise dominance. At 5 dB SNR, P_d increases significantly, showing improved target signal extraction. At 10 dB SNR, the method achieves high P_d, even for low P_f, indicating enhanced signal quality in reduced noise conditions.

VI. Conclusion

This paper investigates the role of RIS in enhancing detection performance within a mono-static NLOS radar system, specifically targeting multipath environments. Employing a manifold gradient descent approach, we show that the proposed method mitigates the degradation caused by multipath propagation, achieving a more robust detection performance than conventional methods, especially under strong multipath conditions. Simulation results validate the theoretical analysis, demonstrating the method's resilience to varying angular spread. The applicability of the proposed approach to complex signal environments underscores its practical potential in multipath-rich scenarios, where traditional techniques may be inadequate. Future work will focus on adaptive RIS configurations for dynamic environments to further optimize detection and energy efficiency.

References

[1] M. A. ElMossallamy, H. Zhang, L. Song, K. G. Seddik, Z. Han, and G. Y. Li, "Reconfigurable intelligent surfaces for wireless communications: Principles, challenges, and opportunities," *IEEE Transactions on Cognitive Communications and Networking*, vol. 6, no. 3, pp. 990–1002, 2020.

[2] Y. Liu, X. Liu, X. Mu, T. Hou, J. Xu, M. Di Renzo, and N. Al-Dhahir, "Reconfigurable intelligent surfaces: Principles and opportunities," *IEEE communications surveys & tutorials*, vol. 23, no. 3, pp. 1546–1577, 2021.

[3] W. Lu, B. Deng, Q. Fang, X. Wen, and S. Peng, "Intelligent reflecting surface-enhanced target detection in MIMO radar," *IEEE Sensors Letters*, vol. 5, no. 2, pp. 1–4, 2021.

[4] C. Pan, H. Ren, K. Wang, J. F. Kolb, M. Elkashlan, M. Chen, M. Di Renzo, Y. Hao, J. Wang, A. L. Swindlehurst *et al.*, "Reconfigurable intelligent surfaces for 6G systems: Principles, applications, and research directions," *IEEE Communications Magazine*, vol. 59, no. 6, pp. 14–20, 2021.

[5] P. Wang, J. Fang, H. Duan, and H. Li, "Compressed channel estimation for intelligent reflecting surface-assisted millimeter wave systems," *IEEE Signal Processing Letters*, vol. 27, pp. 905–909, 2020.

[6] A. Diaz-Rubio, S. Kosulnikov, and S. A. Tretyakov, "On the integration of reconfigurable intelligent surfaces in real-world environments: A convenient approach for estimation reflection and transmission," *IEEE Antennas and Propagation Magazine*, vol. 64, no. 4, pp. 85–95, 2022.

[7] A. Aubry, A. De Maio, and M. Rosamilia, "Reconfigurable intelligent surfaces for N-LOS radar surveillance," *IEEE Transactions on Vehicular Technology*, vol. 70, no. 10, pp. 10 735–10 749, 2021.

[8] C. Ozturk, M. F. Keskin, H. Wymeersch, and S. Gezici, "RIS-aided near-field localization under phase-dependent amplitude variations," *IEEE Transactions on Wireless Communications*, 2023.

[9] A. Araghi, M. Khalily, M. Safaei, A. Bagheri, V. Singh, F. Wang, and R. Tafazolli, "Reconfigurable intelligent surface (RIS) in the sub-6 ghz band: Design, implementation, and real-world demonstration," *IEEE Access*, vol. 10, pp. 2646–2655, 2022.

[10] Z. Esmaeilbeig, K. V. Mishra, and M. Soltanalian, "IRS-aided radar: Enhanced target parameter estimation via intelligent reflecting surfaces," in *2022 IEEE 12th Sensor Array and Multichannel Signal Processing Workshop (SAM)*. IEEE, 2022, pp. 286–290.

[11] S. Buzzi, E. Grossi, M. Lops, and L. Venturino, "Foundations of MIMO radar detection aided by reconfigurable intelligent surfaces," *IEEE Transactions on Signal Processing*, vol. 70, pp. 1749–1763, 2022.

[12] E. Grossi, H. Taremizadeh, and L. Venturino, "Radar target detection and localization aided by an active reconfigurable intelligent surface," *IEEE Signal Processing Letters*, 2023.

[13] Z. Xie, L. Wu, J. Zhu, M. Lops, X. Huang, and B. Shankar, "RIS-aided radar for target detection: Clutter region analysis and joint active-passive design," *IEEE Transactions on Signal Processing*, 2024.

[14] F. Wang, H. Li, and J. Fang, "Joint active and passive beamforming for IRS-assisted radar," *IEEE Signal Processing Letters*, vol. 29, pp. 349–353, 2021.

[15] F. Wang, A. L. Swindlehurst, and H. Li, "Detection performance of RIS-Aided MIMO radar with asynchronous propagation," in *2023 IEEE International Workshop on Computational Advances in Multi-Sensor Adaptive Processing (CAMSAP 2023), DECEMBER 10-13, 2023, LOS SUEÑOS, COSTA RICA*, 2023.

[16] B. Wang, H. Li, S. Shen, Z. Cheng, and B. Clerckx, "A dual-function radar-communication system empowered by beyond diagonal reconfigurable intelligent surface," *IEEE Transactions on Communications*, 2024.

[17] H. Luo, Y. Wang, D. Luo, J. Zhao, H. Wu, S. Ma, and F. Gao, "Integrated sensing and communications in clutter environment," *IEEE Transactions on Wireless Communications*, 2024.

[18] I. Yildirim, A. Uyrus, and E. Basar, "Modeling and analysis of reconfigurable intelligent surfaces for indoor and outdoor applications in future wireless networks," *IEEE Transactions on Communications*, vol. 69, no. 2, pp. 1290–1301, 2020.

[19] C. Zeng, Y. Liang, and H. Li, "Joint active and passive beamforming for NLOS target detection in RIS-assisted mono-static radar," in *2024 Asilomar Conference on Signals, Systems, and Computers, Pacific Grove, CA, USA, Oct.*, 2024.

[20] F. Wang, H. Li, and A. L. Swindlehurst, "Clutter suppression for target detection using hybrid reconfigurable intelligent surfaces," in *2023 IEEE Radar Conference (RadarConf23), May 1-5, 2023, San Antonio, Texas*, 2023, pp. 1–5.

[21] K. Alhujaili, V. Monga, and M. Rangaswamy, "Transmit MIMO radar beampattern design via optimization on the complex circle manifold," *IEEE Transactions on Signal Processing*, vol. 67, no. 13, pp. 3561–3575, 2019.

[22] P.-A. Absil, R. Mahony, and R. Sepulchre, *Optimization algorithms on matrix manifolds*. Princeton University Press, 2008.

[23] N. Boumal, B. Mishra, P.-A. Absil, and R. Sepulchre, "Manopt, a Matlab toolbox for optimization on manifolds," *The Journal of Machine Learning Research*, vol. 15, no. 1, pp. 1455–1459, 2014.